

Activation cross sections of proton induced nuclear reactions on gold up to 65 MeV

F. Ditrói^{a,*}, F. Tárkányi^a, S. Takács^a, A. Hermanne^b

^a*Institute for Nuclear Research, Hungarian Academy of Sciences (ATOMKI), Debrecen, Hungary*

^b*Cyclotron Laboratory, Vrije Universiteit Brussel (VUB), Brussels, Belgium*

^c*Institute of Physics and Power Engineering (IPPE), Obninsk, Russia*

^d*Cyclotron Radioisotope Center (CYRIC), Tohoku University, Sendai, Japan*

Abstract

Activation cross sections of proton induced reactions on gold for production of ^{197m,197g,195m,195g,193m,193g,192}Hg, ^{196m,196g(cum),195g(cum),194,191(cum)}Au, ^{191(cum)}Pt and ¹⁹²Ir were measured up to 65 MeV proton energy, some of them for the first time. The new data are in acceptably good agreement with the recently published earlier experimental data in the overlapping energy region. The experimental data are compared with the predictions of the TALYS 1.6 (results in TENDL-2015 on-line library) and EMPIRE 3.2 code.

Keywords: natural gold target, activation cross section, Hg, Au, Pt and Ir radioisotopes, physical yield, medical and industrial applications

1. Introduction

The experimental proton and deuteron activation cross section data on gold are important in different application fields. Out of the reaction products the radionuclides of mercury are used in monitoring the distribution and the accumulation of mercury in different parts of the body and to study mercury transformations in environmental systems. The accelerator-produced isomers are broadly used in diagnostic medical applications: ^{197m,g}Hg appear to be new potential candidates for therapy. For investigation of specimens containing metallic gold and gold alloys, the longer-lived ^{198g}Au ($T_{1/2} = 2.7$ d) and ^{196g}Au ($T_{1/2} = 6.2$ d) are suitable. Furthermore, experimental studies of the isomers and comparison of the results with nuclear reaction model calculations significantly assist to further development of nuclear reaction theories. We earlier published results of investigations on gold activation cross sections where the different applications were discussed in more detail (IAEA-NDS, 2010; Szelecsényi et al., 1996, 1997; Tárkányi et al., 2011, 2015). The present data are produced in the frame of a systematic study of excitation functions of light charged particles. Our earlier investigation on proton induced activation on gold

was limited to 30 MeV incident particle energy (Szelecsényi et al., 1996). This recent investigation is dedicated mainly to the determination of excitation functions on gallium up to 65 MeV and ⁶⁴Ni up to 30 MeV (Amjed et al., 2014; Hermanne et al., 2015), we have used Au-foils as backing of electrodeposited GaNi and ⁶⁴Ni targets. As during the evaluation of the gamma spectra we got valuable information on activation cross sections also on gold, we decided to share the new information with the public.

2. Earlier experimental data

The main goal of the present work was to extend the energy range of the experimental data for cross sections of radioisotopes produced from gold by proton activation. Besides this goal we could also clarify the discrepancies occur between the relatively large number of data sets from different laboratories, as well as provide further input data for nuclear reaction model code development. Due to different factors (monoisotopic target, easy target preparation, importance of proton activation data for different applications, easy measurable isomeric ratios, etc.) there is a relatively large set of experimental data available in the literature on proton induced activation cross sections on gold. When one overviews the years of the previous measurements,

*Corresponding author: ditroi@atomki.hu

target preparation methods, irradiation circumstances, beam current measurements methods (monitoring), γ -spectrometry tools and the overall result parameters (in the last column of Table 1), one can have a preliminary impression about the quality of the particular data sets. This information can later be used by judging the goodness of the agreements. We collected the results related to the present study in Table 1.

3. Experiment and data evaluation

The experiment was performed using the activation method, stacked foil irradiation technique and off-line high resolution gamma-ray spectrometry. Cross section data were deduced relative to the chosen monitor reactions, re-measured simultaneously over the whole covered energy range. Two stacks were irradiated at an external beam line of the Cyclone110 cyclotron of the Universit   Catholique in Louvain la Neuve (LLN) with a 65 MeV proton beam. The first stack was irradiated at 84 nA for 1 h. It contained a sequence of groups of Al (151.1 μm), Hf (10.54 μm), Al (56.6 μm), Al (26.9 μm) and GaNi alloy layer (17.7 or 15.9 μm) electrodeposited on 25 μm Au foils. The energy range covered by the 18 Au targets was 46.9-63.5 MeV. The second stack contained 12 groups of W (21.3 μm), Al (250 μm) and 13.35 μm GaNi alloy electrodeposited on 13.35 μm Cu, Al (250 μm) followed by 17 blocks of 23.1 μm Au, 125 μm Al, 21.3 μm W, 250 μm Al, 13.2 mm GaNi on 12.5 μm Cu and 125 μm Al foils. The energy range of the 17 Au foils was 47.15-23.1 MeV. The stack was irradiated at 35 nA intensity for 1 h. An additional stack was irradiated at the external beam line of VUB CGR 560 cyclotron (Brussels) at 90 nA for 1 hour with a 33.7 MeV incident proton beam. This consisted of 7 groups of Al (11 μm), In (116 μm), Al (50 μm), Ti (10.9 μm) followed by 11 groups of Au (23.1 μm), Al (11 μm), In (116 μm), Al (50 μm), Ti (10.9 μm) The energy range of 11 Au foils was on 7.2 -25.2 MeV. The targets were mounted in Faraday cup like target holders provided with a long collimator. No chemical separation was used. Gamma-spectra were measured with Canberra HPGe detectors, coupled with plug-in MCA computer card controlled by the Genie2000 software. Four or five series of gamma spectra were measured to follow the decay. The spectra were evaluated by an iterative method using the Genie 2000 or Forgamma (Canberra, 2000; Sz  kely, 1985) codes. The used decay data and the Q values of the contributing reactions are collected in Table 2. The decay data were taken from the on-line version NUDAT (NuDat, 2014), the reaction Q-values are obtained from the Q value calculator (Prity-

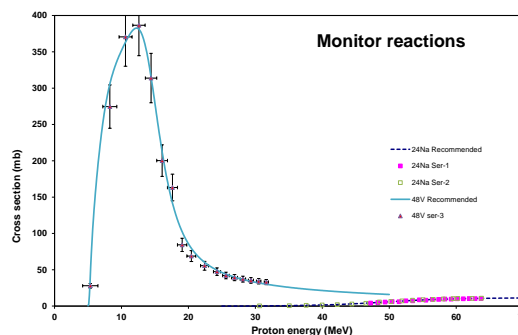


Figure 1: Illustration of agreement of simultaneously measured experimental data of $^{27}\text{Al}(p,x)^{24}\text{Na}$ and $^{nat}\text{Ti}(p,x)^{48}\text{V}$ monitor reactions in comparison with the recommended values to monitor of the proton beam parameters through the irradiated stacks

chenko and Sonzogni, 2003). The simultaneously measured excitation functions of the monitor reactions are shown in Fig. 1 in comparison with the recommended data (T  rk  nyi et al., 2001). In the high energy irradiations the $^{27}\text{Al}(p,x)^{22,24}\text{Na}$ monitor reactions were used, at low energy the $^{nat}\text{Ti}(p,x)^{48}\text{V}$ reaction. The beam energies in targets (preliminary) were determined by using a home-made code based on the tables and coefficients given in (Andersen and Ziegler, 1977) and corrected according to the results of the fitted monitor reactions (final) (T  rk  nyi et al., 1991). Uncertainty of energy was obtained taking into account cumulative effects of possible uncertainties (primary energy, target thickness, energy straggling, correction to monitor reaction). As Au is monoisotopic, so called isotopic cross sections were determined. Due to the complex gamma spectra, the large number of products and their different half-lives, use of experimental data in literature and of theoretical results (tendency, shape, magnitude) help significantly for data evaluation. Uncertainty of cross sections was determined by taking square root from the sum in quadrature of all individual contributions (International-Bureau-of-Weights-and-Measures, 1993): beam current (7 %), beam-loss corrections (max. 1.5 %), target thickness (1 %), detector efficiency (5 %), photo peak area determination and counting statistics (1-20

4. Comparison with nuclear model calculations

The cross-sections of the investigated reactions were compared with the data given in the on-line TENDL-2015 (Koning et al., 2015) library. This library is based

on both default and adjusted TALYS (1.6) calculations (Koning and Rochman, 2012). The calculations we made by EMPIRE 3.2 (Herman et al., 2007)(version Malta (Herman et al., 2012)) are also presented and compared with the experimental results. In the case of TENDL and EMPIRE the same strategy was followed, i.e. all possible contributions were calculated and added in the final results (if it was possible).

5. Cross sections

The experimental cross section data and the comparison with the theoretical results of the TENDL-2014 and TENDL-2015 calculations are shown in Figs. 2-15. The results of the previous version of TENDL is presented in order to demonstrate the improvement in the TALYS calculations. The numerical data are collected in Table 3. The cross section values of mercury radionuclides are due to direct production via (p,xn) reactions. The gold radio-products are produced directly via (p,pxn) reactions and/or additionally through the decay of isobaric parent mercury radioisotopes (cumulative). The ground state of these radioisotopes can additionally be populated through the isomeric transition of the meta-stable state. The cross section is marked with (m+) when the half-life of the isomeric state is significantly shorter than that of the ground state and the cross sections for the production of ground state were deduced from spectra measured after nearly complete decay of the isomeric state.

5.1. Production of mercury radioisotopes

5.1.1. Cross sections for the $^{197}\text{Au}(p,n)^{197m}\text{Hg}$ reaction

The 23.8 h isomeric state decays for 91.4 % to the 64.1 h half-life ground state with emission of a 133.98 keV gamma-line and for the rest to stable ^{197}Au by EC. The production cross sections of the ^{197m}Hg are shown in Fig. 2, together with the earlier experimental results and theoretical estimations in TENDL-2014 and 2015. There is rather good agreement with earlier experimental data except for the studies of (Satheesh et al., 2012) and (Hansen et al., 1962). Unrealistic values for TENDL above 12 MeV can be observed. There are no significant differences between the consecutive TENDL versions. EMPIRE gives much better approximation, especially under 10 MeV and above 20 MeV, it gives also reliable maximum position but overestimates the maximum value.

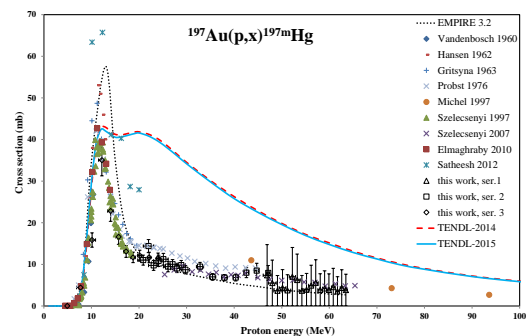


Figure 2: Excitation functions of the $^{197}\text{Au}(p,n)^{197m}\text{Hg}$ reaction in comparison with literature values and theoretical results from TENDL-2014 and 2015

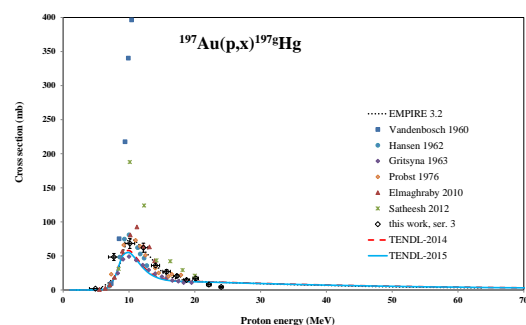


Figure 3: Excitation functions of the $^{197}\text{Au}(p,n)^{197g}\text{Hg}$ reaction in comparison with literature values and theoretical results from TENDL-2014 and 2015

5.1.2. Cross sections for the $^{197}\text{Au}(p,n)^{197g}\text{Hg}$ reaction

The 64.1 h ground state is produced directly via (p,n) reaction and through 91.4 % decay of the isomeric state ($T_{1/2} = 23.8$ h). The experimental data for direct production are shown in Fig. 3. There are large disagreements between the experimental data from the different authors due to several effects: low gamma-energy, weak gamma-lines and separation of the contribution from the decay of isomeric state. The TENDL-2014 and 2015 values seem to give a good description of the shape and the maximum cross section value is near to an average of the experimental ones. The approximation of EMPIRE is better also in this case.

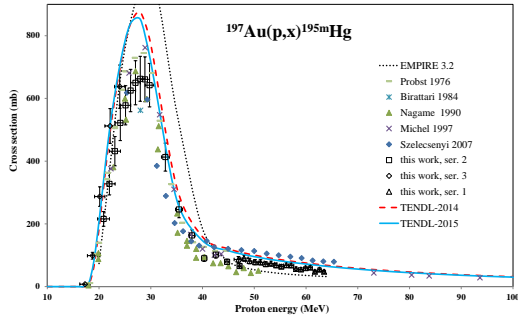


Figure 4: Excitation functions of the $^{197}\text{Au}(p,3n)^{195m}\text{Hg}$ reaction in comparison with literature values and theoretical results from TENDL-2014 and 2015

5.1.3. Cross sections for the $^{197}\text{Au}(p,3n)^{195m}\text{Hg}$ reaction

The radionuclide ^{195}Hg has two states: a longer-lived high spin isomer (^{195m}Hg , $T_{1/2} = 41.6$ h, $I^\pi = 13/2^+$) and the shorter-lived ground state ^{195g}Hg ($T_{1/2} = 10.53$ h, $I^\pi = 1/2^-$). We obtained production cross sections for both states. The experimental and the theoretical data for the longer-lived isomeric state are shown in Fig. 4. The agreement is acceptably good between experimental data. The TENDL-2014 and 2015 calculations slightly overestimate the experiments, but the prediction is acceptably good. There is no significant difference between the TENDL versions. Now the overestimation of EMPIRE is strong between 28 and 40 MeV, but its approximation is better at the remaining energy regions.

5.1.4. Cross sections for the $^{197}\text{Au}(p,3n)^{195g}\text{Hg}$ reaction

The 10.53 h ground state is produced directly via (p,n) reaction and through IT 54.2 % internal decay of the isomeric state (41.6 h). Figure 5 shows the direct production cross sections obtained after separation of possible contributions of isomeric state decay. The experimental data are very scattered above 40 MeV. The almost identical TENDL versions give good estimation only up to 22 MeV, above this value strongly underestimate and also their maximum energy is shifted downwards. EMPIRE gives better approximation regarding to the maximum position and also the values above it, but underestimates the maximum value similarly to TENDL.

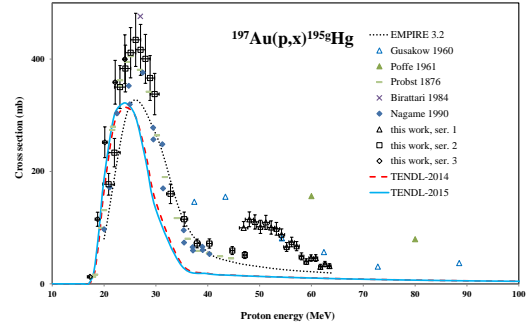


Figure 5: Excitation functions of the $^{197}\text{Au}(p,3n)^{195g}\text{Hg}$ reaction in comparison with literature values and theoretical results from TENDL-2014 and 2015

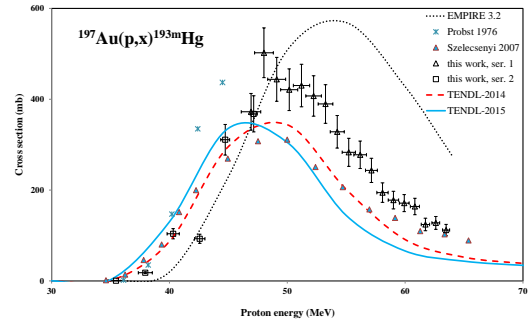


Figure 6: Excitation functions of the $^{197}\text{Au}(p,5n)^{193m}\text{Hg}$ reaction in comparison with literature values and theoretical results from TENDL-2014 and 2015

5.1.5. Cross sections for the $^{197}\text{Au}(p,5n)^{193m}\text{Hg}$ reaction

The radionuclide ^{193}Hg has two states: a longer-lived high spin isomer (^{193m}Hg , $T_{1/2} = 11.8$ h, $I^\pi = 13/2^-$) and the shorter-lived ground state ^{193g}Hg ($T_{1/2} = 3.8$ h, $I^\pi = 3/2^-$). The experimental and theoretical excitation functions for the metastable state are shown in Fig. 6. Only two earlier experimental data sets were found presenting somewhat lower values confirmed by the TENDL-2014 and 2015 results. In this case EMPIRE is shifted and also overestimates.

5.1.6. Cross sections for the $^{197}\text{Au}(p,5n)^{193g}\text{Hg}$ reaction

The experimental excitation function for direct production of ^{193g}Hg , after correction for contribution

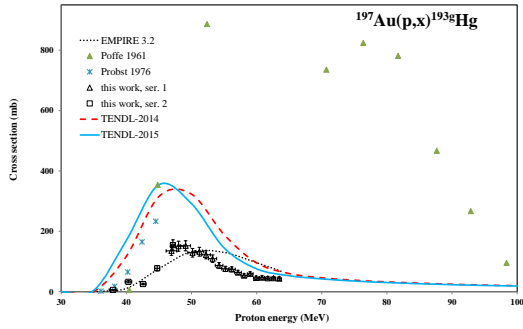


Figure 7: Excitation functions of the $^{197}\text{Au}(p,5n)^{193g}\text{Hg}$ reaction in comparison with literature values and theoretical results from TENDL-2014 and 2015

from isomeric state decay (IT 7.2 %) are shown in Fig. 7. Only two earlier experimental data sets were found presenting significantly higher and scattered values. TENDL-2014 and 2015 confirm the shape of our new results but the predicted maximum value is 100 % higher. In this case the prediction of EMPIRE can be considered as better.

5.1.7. Cross sections for the $^{197}\text{Au}(p,6n)^{192}\text{Hg}$ reaction

The experimental and the TENDL data for production of ^{192}Hg ($T_{1/2} = 4.85$ h) are shown in Fig 8. Our new data are in good agreement with the TENDL-2014 prediction, but differ significantly from the single literature data. The new TENDL-2015 gives a downwards shift in energy, which is not confirmed by our new experimental results. The EMPIRE code fails to give an acceptable approximation in this case.

5.2. Production of gold radioisotopes

Due to the similar half-lives of the parent Hg radioisotopes and the long cooling time before the first gamma spectra (large contribution from the decay already in the first spectra) we decided not to deduce independent cross sections for production ^{193}Au and ^{192}Au ($T_{1/2} = 17.65$ h and 4.94 h respectively).

5.2.1. Cross sections for the $^{197}\text{Au}(p,pn)^{196m2}\text{Au}$ reaction

We could measure the cross section data for formation of the long-lived, high spin, isomeric state $^{196m2}\text{Au}$ ($T_{1/2} = 9.6$ h, 12-, IT 100 %). No earlier experimental

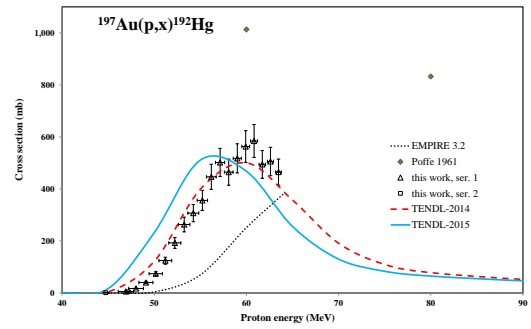


Figure 8: Excitation functions of the $^{197}\text{Au}(p,6n)^{192}\text{Hg}$ reaction in comparison with literature values and theoretical results from TENDL-2014 and 2015

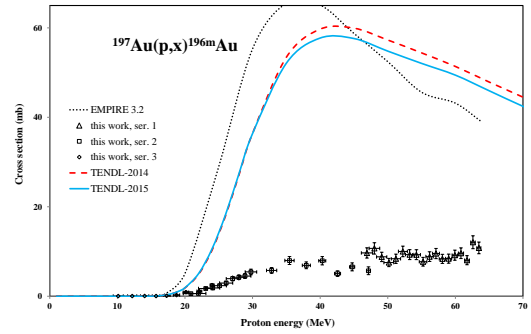


Figure 9: Excitation functions of the $^{197}\text{Au}(p,pn)^{196m2}\text{Au}$ reaction in comparison with literature values and theoretical results from TENDL-2014 and 2015

data were found in the literature (Fig. 9). The TENDL-2014 and 2015 values are 6 times higher near the maximum. EMPIRE gives similarly unacceptable result.

5.2.2. Cross sections for the $^{197}\text{Au}(p,pn)^{196g}\text{Au}$ reaction

The experimental results for direct production of the ^{196g}Au ground state ($T_{1/2} = 6.1669$ d), after correction for contribution of 100 % isomeric transitions from $^{196m2}\text{Au}$ but including the total decay of the direct formation of the 8.2 sec $^{197m1}\text{Au}$ and the 100 % isomeric transitions from $^{196m2}\text{Au}$ ($T_{1/2} = 9.6$ h), are shown in Fig. 10. (^{196}Au (cum)). The rather large number of experimental data sets are showing acceptably good agreement. TENDL-2014 and 2015 are slightly higher than all of the experimental values. EMPIRE underestimates

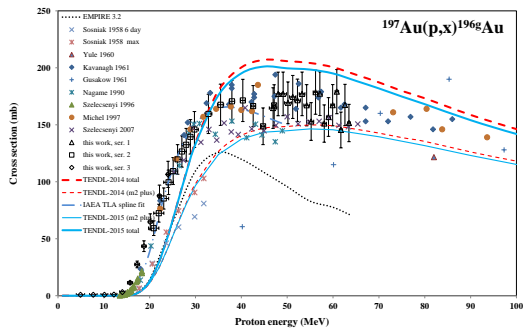


Figure 10: Excitation functions of the $^{197}\text{Au}(p,pn)^{196g}\text{Au}$ reaction in comparison with literature values and theoretical results from TENDL-2014 and 2015

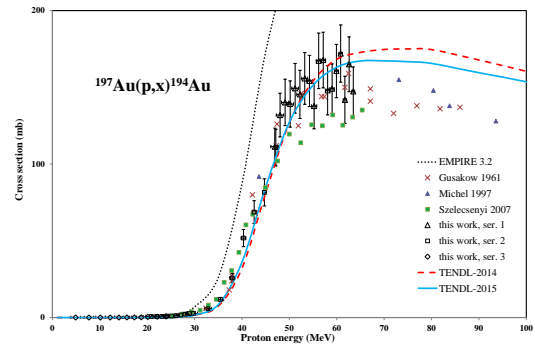


Figure 12: Excitation functions of the $^{197}\text{Au}(p,p3n)^{194}\text{Au}$ reaction in comparison with literature values and theoretical results from TENDL-2014 and 2015

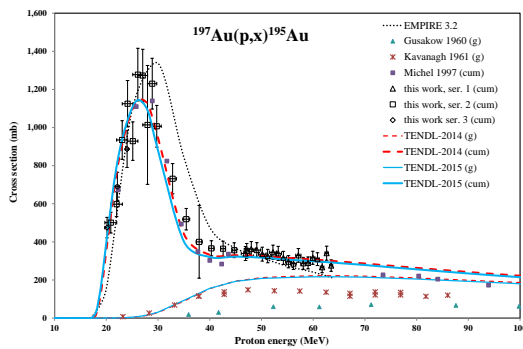


Figure 11: Excitation functions of the $^{197}\text{Au}(p,x)^{195}\text{Au}(\text{cum})$ and $^{197}\text{Au}(p,x)^{195g}\text{Au}$ reactions in comparison with literature values and theoretical results from TENDL-2014 and 2015

in spite of the inclusion of the $^{197m1}\text{Au}$ contribution.

5.2.3. Cross sections for the $^{197}\text{Au}(p,x)^{195g}\text{Au}$ reaction

We deduced cumulative production cross of ^{195g}Au ($T_{1/2} = 186.09$ d), which includes contribution from direct production, from the short-lived ^{195m}Au isomeric state ($T_{1/2} = 30.5$ s, IT 100 %) and from the decay of the isomeric states of parent $^{195m,g}\text{Hg}$ ($T_{1/2} = 41.06$ h and 10.53 h). Our cross section data for the cumulative production (cum) and the literature results for the direct (g) or cumulative (cum) production of the ground state are shown in Fig. 11. The values of TENDL-2014 and 2015 for cumulative production follow closely the experimental data. EMPIRE prediction is shifted and gives some overestimation between 25 and 45 MeV.

5.2.4. Cross sections for the $^{197}\text{Au}(p,p3n)^{194}\text{Au}$ reaction

The direct production cross sections of ^{194}Au ($T_{1/2} = 38.02$ h) are shown in Fig. 12 in comparison with the earlier experimental data. On the basis of the theoretical cross section of the parent ^{194}Hg and taking into account its very long half-life the contribution from the decay of ^{194}Hg ($T_{1/2} = 444$ a) in our experimental circumstances and data uncertainties can be neglected. The TENDL-2014 and 2015 predictions follow our experimental results. A strong overestimation can be observed by EMPIRE above 30 MeV.

5.2.5. Cross sections for the $^{197}\text{Au}(p,x)^{191}\text{Au}$ reaction

The measured cumulative cross sections of ^{191}Au ($T_{1/2} = 3.18$ h) contain the direct production and production through the complete decay of the parent ^{191}Hg ($T_{1/2} = 50.58$ min) (Fig. 13). No earlier experimental data were found in the literature. Our new data are in good agreement with the TENDL-2014 prediction. In this case the new TENDL-2015 shifted the maximum towards lower energies, which is not confirmed by the experiment. The reason of the strong underestimation of EMPIRE is that the production is mainly fed by the ^{191}Hg decay, which was not included in the EMPIRE calculation, because of the code failure by large number of emitted particles at higher energies.

5.3. Production of platinum radioisotopes

5.3.1. Cross sections for the $^{197}\text{Au}(p,x)^{191}\text{Pt}$ reaction

The measured cumulative cross sections of ^{191}Pt ($T_{1/2} = 2.802$ d) (cum = direct ^{191}Pt + decay of ^{191}Au + decay of ^{191}Hg) are practically identical with the production cross sections of ^{191}Au (Fig. 14, see also Fig. 13),

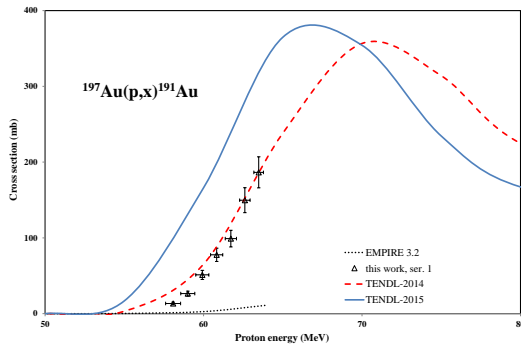


Figure 13: Excitation functions of the $^{197}\text{Au}(p,x)^{191}\text{Au}$ reaction in comparison with literature values and theoretical results from TENDL-2014 and 2015

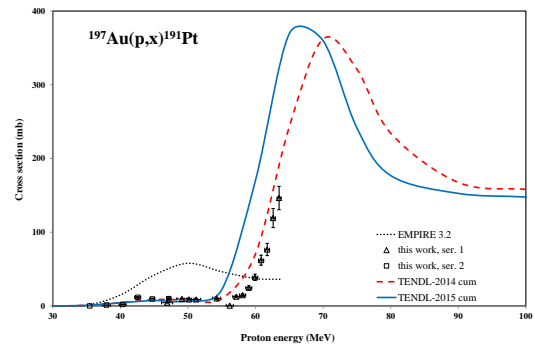


Figure 15: Excitation functions of the $^{197}\text{Au}(p,x)^{191}\text{Pt}$ reaction in comparison with literature values and theoretical results from TENDL-2014 and 2015

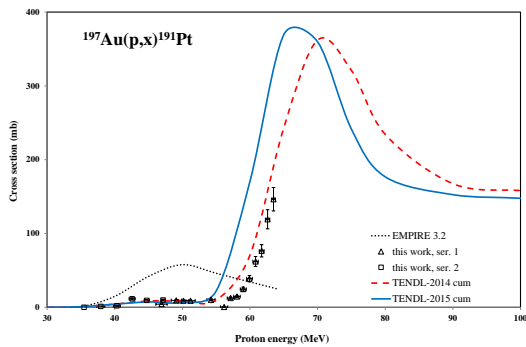


Figure 14: Excitation functions of the $^{197}\text{Au}(p,x)^{191}\text{Pt}(\text{cum})$ reaction in comparison with theoretical results from TENDL-2014 and 2015

indicating the low contribution from the direct production as confirmed by the TENDL-2014 results. TENDL-2015 is not confirmed by our new experimental results again. No earlier experimental data were found in the literature. The EMPIRE prediction disagrees.

5.4. Production of iridium radioisotopes

5.4.1. Cross sections for the $^{197}\text{Au}(p,x)^{192}\text{Ir}$ reaction

The ground state of ^{192}Ir is a closed radioisotope with three longer-lived isomeric states: a very long-lived, high spin, isomer $^{192m2}\text{Ir}$ ($T_{1/2} = 241$ a, $I^\pi = 11^-$), a short-lived, low spin, isomeric state $^{192m1}\text{Ir}$ ($T_{1/2} = 1.45$ min, $I^\pi = 1^-$) and the ground state ^{192g}Ir ($T_{1/2} = 73.829$ d, $I^\pi = 4^+$). The measured cross sections (Fig. 15) contain the direct production and production through

the decay of the short half-life isomeric state. Under the used experimental circumstances, the contribution through the decay of the long-lived isomeric does not play a role, so it was neglected. The agreement with the data of (Michel et al., 1997) is acceptable, the TENDL versions strongly underestimate the experimental values and do not predict the trend of the experimental curves. The EMPIRE strongly overestimates from the threshold.

6. Integral yields

From excitation functions integral thick target yields, obtained by Spline fit to our experimental cross section data, were calculated and shown in Fig. 16 as a function of the energy for the radionuclides with known applications ($^{197m,g}\text{Hg}$, $^{195m,g}\text{Hg}$ and $^{196m,g}\text{Au}$). Experimental thick target yields exist in the literature (Abe et al., 1984; Birattari and Bonardi, 1980; Dmitriev, 1983; Dmitriev and Molin, 1981), which are also presented in Fig. 16. For ^{197m}Hg our results are slightly lower than the results of (Abe et al., 1984) and much larger than the single data point of (Birattari and Bonardi, 1980) at 16 MeV. In the case of ^{197g}Hg the single data point of (Dmitriev and Molin, 1981) is slightly larger than our value, while the curve given by Birattari et al. is larger and the single data point of Abe et al. is lower than our values. In the case ^{195m}Hg the data of Birattari et al. run slightly under our results, above 20 MeV the agreement is rather acceptable. The results for the ground state ^{195g}Hg show similar behavior as the metastable state. In the case of ^{196m}Au the previous data of Birattari et al. are

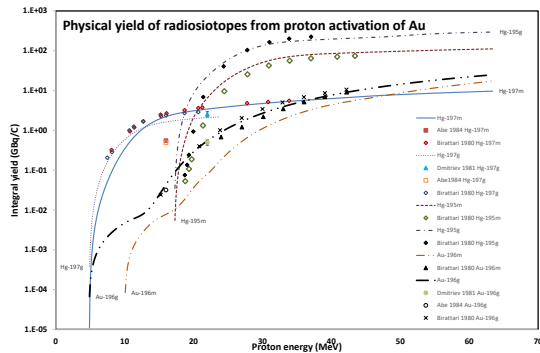


Figure 16: Integral yields calculated from the measured excitation functions compared with the literature data

above our results, while by the ground state the agreements with the single points of Dmitriev and Molin at 22 MeV and Abe et al. at 16 MeV as well as with the curve from Birattari et al. are excellent.

7. Applications

Possible medical applications for therapeutic nuclear medicine were recently discussed in detail in our works on activation cross sections of deuteron induced reactions on gold published recently (Tárkányi et al., 2011, 2015). Here we discuss only the relevance for applications in the thin layer activation technique (TLA) and for beam monitoring.

7.1. Thin layer activation

For TLA investigation of specimens containing metallic gold or gold alloys, only the longer-lived ^{198g}Au ($T_{1/2} = 2.7$ d) and ^{196g}Au ($T_{1/2} = 6.2$ d) are suitable among the reaction products studied here and in our previous work (Tárkányi et al., 2015). Application of ^{196g}Au was already presented in detail in the TLA data library of the IAEA (IAEA-NDS, 2010). We compare the IAEA recommended data with our new results in Fig. 10. The comparison shows that the experimental data should be refitted, especially above 45 MeV.

7.2. Beam monitoring

A thin layer of gold is frequently used as target backing material due to its favorable physical and chemical properties. When irradiating the target a few reactions are induced simultaneously in the gold-backing resulting in radioproducts suitable for beam energy and intensity determination. The quality of the gold cross section

data however is still not satisfactory. Among the investigated reactions the reactions resulting in ^{197m}Hg (above 10 MeV), ^{195m}Hg (above 20 MeV), ^{196g}Au (above 20 MeV), ^{195}Au (above 20 MeV, long measurement is necessary) and ^{194}Au (above 40 MeV) could be used (see Figures 2, 4, 10, 11 and 12).

8. Summary and conclusion

Excitation functions of $^{197m,197g,195m,195g,193m,193g,192}\text{Hg}$, $^{196m,196g(cum),195g(cum),194,191(cum)}\text{Au}$, $^{191(cum)}\text{Pt}$ and ^{192}Ir nuclear reactions are reported up to 65 MeV, some of them for the first time, relative to well documented monitor reactions. Detailed compilation of earlier experimental data was performed. The agreement is acceptable except for a few reactions. The TENDL-2014 describes well the experiments except for a few isomeric states, while TENDL-2015 shows a little worse prediction than the previous TENDL version. The EMPIRE codes gives better predictions mainly in the cases of a few particle emissions, but fails when complex emissions are also possible and at higher energies. The extended experimental data base provides a basis for improved model calculations and for applications in radioisotope production, in accelerator technology, in charged particle activation analysis and in thin layer application.

9. Acknowledgements

This work was done in the frame of MTA-FWO (Vlaanderen) research projects. The authors acknowledge the support of research projects and of their respective institutions in providing the materials and the facilities for this work. One of the authors (F. Ditráři) would also acknowledge the support of IAEA and namely to R. Capote and M. Herman for the valuable advices in installing and using the newest EMPIRE code for charged particle reactions.

References

- Abe, K., Iizuka, A., Hasegawa, A., Morozumi, S., 1984. Induced radioactivity of component materials by 16-mev protons and 30-mev alpha-particles. *Journal of Nuclear Materials* 123 (1-3), 972–976.
- Albouy, G., Cohen, J. P., Gusakov, M., Poffe, N., Sergolle, H., Valentin, L., 1963. $R\hat{A}$ eactions (p, 3p3n) entre 30 et 150 mev. *J. Phys. Radium* 24, 67–68.
- Alderliesten, C., Bousshid, O., Jahn, P., Maier-Börlicke, C., 1975. Measurement and hybrid model analysis of (particle,xnyp) excitation functions. Tech. rep.

- Amjed, N., Tárkányi, F., Hermanne, A., Ditrói, F., Takács, S., Hus-sain, M., 2014. Activation cross-sections of proton induced reactions on natural ni up to 65 mev. *Applied Radiation and Isotopes* 92, 73–84.
- Andersen, H. H., Ziegler, J. F., 1977. Hydrogen stopping powers and ranges in all elements. The stopping and ranges of ions in matter, Volume 3. The Stopping and ranges of ions in matter. Pergamon Press, New York.
- Birattari, C., Bonardi, M., 1980. Excitation functions for nuclear reactions (p,xn) and (p,pxn) on targets of gold and study of the production of the ultra-short-lived radioisotope au-195-m. Tech. rep., IFNF.
- Boehm, F., Marmier, P., Preiswerk, P., 1952. Relative cross sections for the excitation of isomers and ground states by (p,n) reaction. *Helvetica Physica Acta* 25, 599.
- Bonardi, M., Birattari, C., 1984. Excitation-functions for the au(p, 3n)hg-195m, hg-195 nuclear-reactions and hg-195m, hg-195/au-195m generator yields. *International Journal of Applied Radiation and Isotopes* 35 (6), 564–564.
- Canberra, 2000. http://www.canberra.com/products/radiochemistry_lab/genie-2000-software.asp.
- Chodil, G., Jopson, R. C., Mark, H., Swift, C. D., Thomas, R. G., Yates, M. K., 1967. (p,n) and (p,2n) cross sections on nine elements between 7.0 and 15.0 mev. *Nuclear Physics A* 93, 648.
- Dmitriev, P. P., 1983. Systematics of nuclear reaction yields for thick target at 22 mev proton energy. *Vop. At. Nauki i Tekhn., Ser. Yadernye Konstanty* 57, 2.
- Dmitriev, P. P., Molin, G. A., 1981. Radioactive nuclide yields for thick target at 22 mev proton energy. *Vop. At. Nauki i Tekhn., Ser. Yadernye Konstanty* 44 (5), 43.
- Elmaghraby, E. K., Hassan, K. F., Omara, H., Saleh, Z. A., 2010. Production of the mercury-197 through proton induced reaction on gold. *Applied Radiation and Isotopes* 68 (9), 1694–1698.
- Gritsyna, V. T., Klyucharev, A. P., Remaev, V. V., Reshetova, L. N., 1963. Ratio of the cross sections for the production of the isomer and ground states of nuclei in the (p,n) reaction at the energies from the threshold to 20 mev. *Soviet Physics - JETP* 17, 1186.
- Gusakow, M., Albouy, G., Poffe, N., Riehl, C., 1961. Reactions (p,pn) a moyenne energie. *J. Phys. Radium* 22, 636.
- Gusakow, M., Legoux, Y., Sergolle, H., 1960. Spallation reaction (p,n+p), (p,2n+p) and (p,3n) on gold. production effective cross section at variation proton energy. *Comptes Rendus De L Academie Des Sciences* 251, 70.
- Hansen, L. F., Jopson, R. C., Mark, H., Swift, C. D., 1962. Ta181(p,n)w181 and au197(p,n)hg197 excitation functions between 4 and 13 mev. *Nuclear Physics* 30, 389.
- Herman, M., Capote, R., Carlson, B. V., Oblozinsky, P., Sin, M., Trkov, A., Wienke, H., Zerkin, V., 2007. Empire: Nuclear reaction model code system for data evaluation. *Nuclear Data Sheets* 108 (12), 2655–2715.
- Herman, M., Capote, R., Sin, M., Trkov, A., Carlson, B., Oblozinsky, P., Mattoon, C., Wienke, H., Hoblit, S., Cho, Y.-S., Plujko, V., Zerkin, V., 2012. Nuclear reaction model code empire-3.2 (malta).
- Hermanne, A., Adam-Rebeles, R., Tarkanyi, F., Takacs, S., Ditrói, F., 2015. Proton and deuteron induced reactions on ga-nat: Experimental and calculated excitation functions. *Nuclear Instruments & Methods in Physics Research Section B-Beam Interactions with Materials and Atoms* 359, 145–154.
- IAEA-NDS, 2010. Thin layer activation (tla) technique for wear measurement.
- International-Bureau-of-Weights-and-Measures, 1993. Guide to the expression of uncertainty in measurement, 1st Edition. International Organization for Standardization, Genève, Switzerland.
- Kavanagh, T. M., Bell, R. E., 1961. Cross sections of (p,pxn) reactions in au-197. *Canadian Journal of Physics* 39, 1172.
- Koning, A. J., Rochman, D., 2012. Modern nuclear data evaluation with the talys code system. *Nuclear Data Sheets* 113, 2841.
- Koning, A. J., Rochman, D., Kopecky, J., Sublet, J. C., Bauge, E., Hilaire, S., Romain, P., Morillon, B., Duarte, H., van der Marck, S., Pomp, S., Sjostrand, H., Forrest, R., Henriksson, H., Cabellos, O., S., G., Leppanen, J., Leeb, H., Plompen, A., Mills, R., 2015. Tendl-2015: Talys-based evaluated nuclear data library.
- Kusch, W., 1975. Isomeric cross-section for au-197(p,n)hg-197m reaction in energy interval 6.5-9.5 mev. *Acta Physica Polonica B* 6 (5), 741–748.
- Michel, R., Bodemann, R., Busemann, H., Daunke, R., Gloris, M., Lange, H. J., Klug, B., Krins, A., Leya, I., Lupke, M., Neumann, S., Reinhardt, H., SchnatzButtgen, M., Herpers, U., Schiekkel, T., Sudbrock, F., Holmqvist, B., Conde, H., Malmberg, P., Suter, M., DittrichHannen, B., Kubik, P. W., Synal, H. A., Filges, D., 1997. Cross sections for the production of residual nuclides by low- and medium-energy protons from the target elements c, n, o, mg, al, si, ca, ti, v, mn, fe, co, ni, cu, sr, y, zr, nb, ba and au. *Nuclear Instruments & Methods in Physics Research Section B-Beam Interactions with Materials and Atoms* 129 (2), 153–193.
- Nagame, Y., Sueki, K., Baba, S., Nakahara, H., 1990. Isomeric yield ratios in proton-, 3-, and alpha-particle-induced reactions on 197au. *Physical Review C* 41 (3), 889–897, pRC.
- NuDat, 2014. Nudat2 database (2.6).
- Pritychenko, B., Sonzogni, A., 2003. Q-value calculator.
- Probst, H. J., Jahn, P., Alderliesten, C., Mayer-Boricke, C., 1997. Experimental cross sections of 197au(p,xn) reactions.
- Satheesh, B., Musthafa, M. M., Singh, B. P., Prasad, R., 2012. Study of isomeric cross-section ratio and pre-equilibrium fraction in proton and alpha particle induced nuclear reactions on au-197. *International Journal of Modern Physics E-Nuclear Physics* 21 (6), Artn 1250059.
- Scholten, B., Qaim, S. M., Stocklin, G., 1994. Radiochemical studies of proton-induced be-7 emission reactions in the energy-range of 40 to 100 mev. *Radiochimica Acta* 65 (2), 81–86.
- Sosniak, J., 1958. Phd thesis., Ph.D. thesis.
- Sudár, S., Qaim, S. M., 2006. Cross sections for the formation of 195hgm,g, 197hgm,g, and 196aum,g in a and 3he-particle induced reactions on pt: Effect of level density parameters on the calculated isomeric cross-section ratio. *Physical Review C* 73 (3), 034613, pRC.
- Székely, G., 1985. Fgm - a flexible gamma-spectrum analysis program for a small computer. *Computer Physics Communications* 34 (3), 313–324.
- Szelecsényi, F., Boothe, T. E., Tavano, E., Fenyvesi, A., Takács, S., Tárkányi, F., 1996. (p,xn) and (p,pn) processes on 197au: New proton monitor reactions up to 30mev.
- Szelecsényi, F., Steyn, G. F., Kovács, Z., van der Walt, T. N., 2008. Application of au+p nuclear reactions for proton beam monitoring up to 70 mev. In: Bersillon, O., Günsing, F., Bange, E. (Eds.), *International Conference on Nuclear Data for Science and Technology*. EDP Sciences, pp. 1259–1262.
- Szelecsényi, F., Takács, S., Fenyvesi, A., Szűcs, Z., Tárkányi, F., Heselius, S. J., Bergman, J., Boothe, T. E., 1997. Study of the au-197(p,pn)au-196m1, au-m2, au-g, au- and au-197(p,n)hg-197m reactions and their application for proton beam monitoring in radioisotope production. *International Conference on Nuclear Data for Science and Technology*, Vol 59, Pt 1 and 2 59, 1483–1485.
- Tárkányi, F., Ditrói, F., Hermanne, A., Takács, S., Király, B., Yamazaki, H., Baba, M., Mohammadi, A., Ignatyuk, A. V., 2011. Activation cross-sections of deuteron induced nuclear reactions on gold up to 40 mev. *Nuclear Instruments & Methods in Physics Research Section B-Beam Interactions with Materials and Atoms* 269 (12), 1389–1400.
- Tárkányi, F., Hermanne, A., Ditrói, F., Takács, S., Rebeles, R. A.,

- Ignatyuk, A. V., 2015. New data on cross-sections of deuteron induced nuclear reactions on gold up to 50 meV and comparison of production routes of medically relevant Au and Hg radioisotopes. *Nuclear Instruments & Methods in Physics Research Section B-Beam Interactions with Materials and Atoms* 362, 116–132.
- Tárkányi, F., Szelecsényi, F., Takács, S., 1991. Determination of effective bombarding energies and fluxes using improved stacked-foil technique. *Acta Radiologica, Supplementum* 376, 72.
- Tárkányi, F., Takács, S., Gul, K., Hermanne, A., Mustafa, M. G., Nortier, M., Obložinsky, P., Qaim, S. M., Scholten, B., Shubin, Y. N., Youxiang, Z., 2001. Beam monitor reactions (chapter 4). charged particle cross-section database for medical radioisotope production: diagnostic radioisotopes and monitor reactions. Tech. rep., IAEA.
- Thomas, R. G., Bartolini, W., 1967. Neutron production in Ag, Ta, Au, Pt, and Pb by the interaction of 7.5-14-MeV protons. *Physical Review* 159, 1022.
- Vandenbosch, R., Huizenga, J. R., 1960. Isomeric cross-section ratios for reactions producing the isomeric pair ^{197m}Hg , ^{197}Hg . *Phys. Rev.* 120, 1313–1318.
- Wu, S., Hsiung, G. Y., Huang, S. L., Liu, Y. C., 1986. Competition effects in proton-induced reactions on ^{65}Cu . *Chinese Journal of Physics* 24, 204.
- Yule, H. P., Turkevich, A., 1960. Radiochemical studies of the (p,pn) reaction in complex nuclei in the 80-450-MeV range. *Physical Review* 118, 1591.

Table 1: Earlier experimental data

Author	Target	Irradiation	Beam current measurement and monitor reaction	Measurement of activity	Reaction Measured quantity Number of measured data points Energy range (MeV)
(Boehm et al., 1952)	Au foil	Cyclotron Single target		GM counter	$^{197m}\text{Hg}/^{197g}\text{Hg}$, σ rat, No.1,6.7 MeV
(Sosniak, 1958)	Au foil 10 and 15 μm	Syncro-cyclotron	$^{12}\text{C}(\text{p,pn})^{11}\text{C}$ $^{19}\text{F}(\text{p,pn})^{18}\text{F}$	Chemical separation Kx, Scint. counter	$^{197}\text{Au}(\text{p,pn})^{196}\text{Au}$, σ , No. 5, 82-426 MeV
(?)	Au foil	Syncro-cyclotron Single target	$^{27}\text{Al}(\text{p,x})^{24}\text{Na}$	Chemical separation Na(I) scintillator	$^{197}\text{Au}(\text{p,3n})^{195g}\text{Hg}(\text{m+})$, σ , No. 1, 155 MeV $^{197}\text{Au}(\text{p,3n})^{197g}\text{Hg}(\text{m+})$, σ , No. 1, 155 MeV
(Yule and Turkevich, 1960)	Au foils 10-25 mg/cm^2	Syncro-cyclotron Single target (recoil catchers)	$^{27}\text{Al}(\text{p,x})^{24}\text{Na}$ $^{12}\text{C}(\text{p,pn})^{11}\text{C}$	Chemical separation Prop. Counter Scint. counter	$^{197}\text{Au}(\text{p,pn})^{196}\text{Au}$, σ , No. 6, 17.7-31.8 MeV
(Vandenbosch and Huizenga, 1960)	Au foils 100-600 μm	Cyclotron Stacked target	Faraday cup	No Chemical separation Na(I) scintillator	$^{197}\text{Au}(\text{p,n})^{197m}\text{Hg}$, ^{197g}Hg , σ and σ_{rat} , No.5,7.3-10.4 MeV
(Gusakow et al., 1960)	Au foil	Syncro-cyclotron Single target	$^{27}\text{Al}(\text{p,x})^{24}\text{Na}$ $^{12}\text{C}(\text{p,pn})^{11}\text{C}$		$^{197}\text{Au}(\text{p,p2n})^{195g}\text{Au}$, σ , No. 9, 35.9-154.8 MeV
(Gusakow et al., 1961)	Au foil	Syncro-cyclotron Single target	$^{27}\text{Al}(\text{p,x})^{24}\text{Na}$ $^{12}\text{C}(\text{p,pn})^{11}\text{C}$	Chemical separation γ -Na(I) scintillator	$^{197}\text{Au}(\text{p,pn})^{196}\text{Au}$, σ , No. 8, 40.2-155.5 MeV $^{197}\text{Au}(\text{p,3n})^{195g}\text{Hg}$, σ , No. 2, 60-80 MeV $^{197}\text{Au}(\text{p,5n})^{193g}\text{Hg}$, σ , No. 18, 40.4-155 MeV $^{197}\text{Au}(\text{p,6n})^{192g}\text{Hg}$, σ , No. 2, 60-80 MeV $^{197}\text{Au}(\text{p,7n})^{191g}\text{Hg}$, σ , No. 2, 60-80 MeV $^{197}\text{Au}(\text{p,7n})^{190g}\text{Hg}$, σ , No. 1, 80 MeV
(?)	Au foil	Syncro-cyclotron Single target	$^{27}\text{Al}(\text{p,x})^{24}\text{Na}$	Chemical separation Na(I) scintillator	$^{197}\text{Au}(\text{p,3n})^{195g}\text{Hg}(\text{m+})$, σ , No. 1, 155 MeV
(Kavanagh and Bell, 1961)	Au foil 20-40 mg/cm^2	Syncro-cyclotron Single target	$^{27}\text{Al}(\text{p,x})^{24}\text{Na}$	Chemical separation Na(I) scintillator	$^{197}\text{Au}(\text{p,pn})^{196}\text{Au}$, σ , No. 26, 18-86 MeV $^{197}\text{Au}(\text{p,p2n})^{195}\text{Au}$, σ , No. 19, 23.2-86 MeV $^{197}\text{Au}(\text{p,p3n})^{194}\text{Au}$, σ , No. 20, 32.4-86 MeV
(Hansen et al., 1962)	Au foil 10 mg/cm^2	Cyclotron stacked foil	Faraday cup	Na(I) scintillator	$^{197}\text{Au}(\text{p,n})^{197g}\text{Hg}$, σ , No. 8, 7-12.7 σ MeV $^{197}\text{Au}(\text{p,n})^{197g}\text{Hg}$, σ , No. 8, 7-12.7 MeV $^{197}\text{Au}(\text{p,n})^{197m}\text{Hg}$, σ , No. 8, 7-12.7 MeV
(Albouy et al., 1963)	Au foil	Syncro-cyclotron Single target	$^{27}\text{Al}(\text{p,x})^{24}\text{Na}$ $^{12}\text{C}(\text{p,pn})^{11}\text{C}$ $^{12}\text{C}(\text{p,pn})^{7}\text{Be}$	Chemical separation Prop. Count	$^{197}\text{Au}(\text{p,x})^{192}\text{Ir}$, σ , No. 9, 44.53-149.66 MeV
(Gritsyna et al., 1963)	Au foil 5-30 mg/cm^2	LINAC Stacked target		Na(I)	$^{197}\text{Au}(\text{p,n})^{197g}\text{Hg}$, σ , No. 13, 8.3-19.5 MeV $^{197}\text{Au}(\text{p,n})^{197m}\text{Hg}$, σ , No. 13, 8.3-19.5 MeV
(Thomas and Bartolini, 1967)	Au foil 2 mg/cm^2	Cyclotron Single target	Faraday cup PP ion chamber Energy range of scattered particles	Neutron Liquid scintillator	$^{197}\text{Au}(\text{p,2n})^{196g}\text{Hg}$, σ , No. 10, 9.7-13.9 MeV $^{197}\text{Au}(\text{p,n})^{196g}\text{Hg} + ^{197}\text{Au}(\text{p,pn})^{196}\text{Au}$, σ , No. 14, 7.6-13.9 MeV
(Chodil et al., 1967)	Au foil 2 mg/cm^2 (2.0 mg/cm^2). Au (2.0 mg/cm^2).	Cyclotron Single target	Faraday cup PP ion chamber Energy range of scattered particles	Neutron Liquid scintillator	$^{197}\text{Au}(\text{p,2n})^{196g}\text{Hg}$, σ , No. 15, 7-15 MeV $^{197}\text{Au}(\text{p,n})^{196g}\text{Hg} + ^{197}\text{Au}(\text{p,pn})^{196}\text{Au}$, σ , No. 15, 7-15 MeV $^{197}\text{Au}(\text{p,x,n})$, σ , No. 20, 7-15 MeV
(Kusch, 1975)	Au foil	Linear accelerator Stacked foil		Ge(Li)	$^{197}\text{Au}(\text{p,n})^{197m}\text{Hg}$, ^{197g}Hg , σ and σ_{rat} , No.6,6.5-9.5 MeV $^{197}\text{Au}(\text{p,n})^{197g}\text{Hg}$, σ , No. 4, 6.5-9.5 MeV
(Alderliesten et al., 1975)	Au foil	Cyclotron		Ge(Li)	
(Probst et al., ????)		Cyclotron Single target	Faraday cup	Ge(Li)	$^{197}\text{Au}(\text{p,n})^{197g}\text{Hg}$, σ , No. 10, 7.3-17.9 MeV $^{197}\text{Au}(\text{p,n})^{197m}\text{Hg}$, σ , No. 31, 6.4-44.6 MeV $^{197}\text{Au}(\text{p,3n})^{195g}\text{Hg}$, σ , No. 20, 17.9-44.6 MeV $^{197}\text{Au}(\text{p,3n})^{195m}\text{Hg}$, σ , No. 20, 17.9-44.6 MeV $^{197}\text{Au}(\text{p,3n})^{194g}\text{Hg}$, σ , No. 10, 26.9-44.6 MeV $^{197}\text{Au}(\text{p,5n})^{193g}\text{Hg}$, σ , No. 5, 36.1-44.9 MeV $^{197}\text{Au}(\text{p,5n})^{193m}\text{Hg}$, σ , No. 5, 36.1-44.9 MeV
(Birattari and Bonardi, 1980)	Au foil 26.23 mg/cm^2	cyclotron	Faraday cup	Ge(Li)	$^{197}\text{Au}(\text{p,n})^{197g}\text{Hg}$, ity , No. 9, 7.4-20.7 MeV $^{197}\text{Au}(\text{p,n})^{197m}\text{Hg}$, ity , No. 12, 8.11-33.9 MeV $^{197}\text{Au}(\text{p,3n})^{195g}\text{Hg}$, ity , No. 10, 18.7-37 MeV $^{197}\text{Au}(\text{p,3n})^{195m}\text{Hg}$, ity , No. 11, 18.8-43.4 MeV $^{197}\text{Au}(\text{p,5n})^{193m}\text{Hg}$, ity , No. 10, 36.4-44.6 MeV $^{197}\text{Au}(\text{p,2n})^{196g}\text{Hg}$, ity , No. 19, 15.2-42.2 MeV $^{197}\text{Au}(\text{p,2n})^{196m2}\text{Hg}$, ity , No. 9, 24-42.2 MeV $^{197}\text{Au}(\text{p,2n})^{194g}\text{Hg}$, ity , No. 5, 30.2-42.2 MeV
(Dmitriev and Molin, 1981)		Cyclotron Stacked target		Ge(Li)	$^{197}\text{Au}(\text{p,pn})^{196}\text{Au}$, ity , No. 1, 22 MeV $^{197}\text{Au}(\text{p,n})^{197g}\text{Hg}$, ity , No. 1, 22 MeV
(Dmitriev, 1983)		Cyclotron Stacked target		Ge(Li)	$^{197}\text{Au}(\text{p,n})^{197g}\text{Hg}$, py , No. 1, 22 MeV $^{197}\text{Au}(\text{p,x})^{196}\text{Au}$, py , No. 1, 22 MeV
(Abe et al., 1984)		Cyclotron	$^{65}\text{Cu}(\text{p,n})^{65}\text{Zn}$	Ge(Li)	$^{197}\text{Au}(\text{p,pn})^{196g}\text{Au}(\text{m+})$, ity , No. 1, 16 MeV $^{197}\text{Au}(\text{p,pn})^{197g}\text{Hg}(\text{m+})$, ity , No. 1, 16 MeV $^{197}\text{Au}(\text{p,pn})^{197g}\text{Hg}$, ity , No. 1, 16 MeV $^{197}\text{Au}(\text{p,pn})^{197m}\text{Hg}$, ity , No. 1, 16 MeV
(Bonardi and Birattari, 1984)	Au foil 26.23 mg/cm^2	cyclotron	Faraday cup	Ge(Li)	$^{197}\text{Au}(\text{p,3n})^{195g}\text{Hg}$, σ , No. 1, 27 MeV $^{197}\text{Au}(\text{p,3n})^{195m}\text{Hg}$, σ , No. 1, 28 MeV
(Wu et al., 1986)	Au foil 200 μm	VdG	Faraday cup	n-Long Counter	$^{197}\text{Au}(\text{p,n})^{197g}\text{Hg}$, σ -rel, No. 1.572-2.594 MeV
(Nagame et al., 1990)	Au foil 5-10 mg/cm^2	Cyclotron		Ge(Li)	$^{197}\text{Au}(\text{p,3n})^{195g}\text{Hg}$, σ , No. 17, 20-40.3 MeV $^{197}\text{Au}(\text{p,3n})^{195m}\text{Hg}$, σ , No. 24, 18-50.8 MeV $^{197}\text{Au}(\text{p,3n})^{195m}\text{Hg}/^{195g}\text{Hg}$, σ_{rat} , No. 14, 20-40.2 MeV $^{197}\text{Au}(\text{p,pn})^{196g}\text{Au}$, σ , No. 15, 13.9-49 MeV $^{197}\text{Au}(\text{p,pn})^{196m}\text{Au}$, σ , No. 13, 20.5-49.1 MeV $^{197}\text{Au}(\text{p,pn})^{196m}\text{Au}/^{196g}\text{Au}$, σ_{rat} , No. 13, 20.1-48.9 MeV

Table 1: continued

Author	Target	Irradiation	Beam current measurement and monitor reaction	Measurement of activity	Reaction Measured quantity Number of measured data points Energy range (MeV)
(Scholten et al., 1994)	Au foil	Cyclotron Stacked foil	$^{nat}\text{Cu}(p,x)^{62,65}\text{Zn}$ $^{27}\text{Al}(p,x)^{22,24}\text{Na}$	Ge(Li)	$^{197}\text{Au}(p,x)^{197}\text{Be}, \sigma, \text{No. } 7, 40-92.9 \text{ MeV}$
(Szelecsényi et al., 1997)	Au foil 49 mg/cm ² 9.4 mg/cm ²	Cyclotron Stacked foil	Faraday	Ge(Li)	$^{197}\text{Au}(p,n)^{197m}\text{Hg}, \sigma, \text{No. } 7, 4.7-18.3 \text{ MeV}$ $^{197}\text{Au}(p,pn)^{196}\text{Au}, \sigma, \text{No. } 24, 13.5-18.3 \text{ MeV}$
(Michel et al., 1997)	Au foil	Cyclotron Synro-cyclotron Stacked foil	$^{nat}\text{Cu}(p,x)^{65}\text{Zn}$ $^{27}\text{Al}(p,x)^{22}\text{Na}$	Ge(Li),HPGe	$^{197}\text{Au}(p,n)^{197g}\text{Hg}, \sigma, \text{No. } 7, 43.6-142 \text{ MeV}$ $^{197}\text{Au}(p,n)^{197m}\text{Hg}, \sigma, \text{No. } 8, 28.9-800 \text{ MeV}$ $^{197}\text{Au}(p,n)^{197m}\text{Hg}, \sigma, \text{No. } 32, 22.3-1600 \text{ MeV}$ $^{197}\text{Au}(p,pn)^{196}\text{Au}, \sigma, \text{No. } 38, 22.3-2600 \text{ MeV}$ $^{197}\text{Au}(p,p2n)^{195}\text{Au}, \sigma, \text{No. } 37, 22.3-2600 \text{ MeV}$ $^{197}\text{Au}(p,p2n)^{194}\text{Au}, \sigma, \text{No. } 31, 43.6-2600 \text{ MeV}$ $^{197}\text{Au}(p,pn)^{191}\text{Pt}, \sigma, \text{No. } 6, 40-2600 \text{ MeV}$ $^{197}\text{Au}(p,pn)^{192}\text{Ir}, \sigma, \text{No. } 32, 4-2600 \text{ MeV}$ and others
(Sudár and Qaim, 2006)	Au foil	Cyclotron Stacked foil	$^{63}\text{Cu}(p,n)^{63}\text{Zn}$ $^{65}\text{Zn}(p,n)^{65}\text{Zn}$	HPGe	$^{197}\text{Au}(p,n)^{197m}\text{Hg}^{197g}\text{Hg}, \sigma, \text{rat. No. } 6, 8.8-18.3 \text{ MeV}$
(Szelecsényi et al., 2008)	Au foil 4.86 μm	Cyclotron Stacked foil	Faraday	HPGe	$^{197}\text{Au}(p,3n)^{195m}\text{Hg}, \sigma, \text{No. } 20, 25.4-85.4 \text{ MeV}$ $^{197}\text{Au}(p,p3n)^{194}\text{Au}, \sigma, \text{No. } 21, 25.4-65.4 \text{ MeV}$ $^{197}\text{Au}(p,5n)^{193m}\text{Hg}, \sigma, \text{No. } 16, 34.6-65.4 \text{ MeV}$ $^{197}\text{Au}(p,n)^{197m}\text{Hg}, \sigma, \text{No. } 21, 25.4-65.4 \text{ MeV}$ $^{197}\text{Au}(p,pn)^{196}\text{Au}, \sigma, \text{No. } 21, 25.4-65.4 \text{ MeV}$
(Elmaghraby et al., 2010)	Au foil 10 μm	Cyclotron Stacked foil	$^{nat}\text{Cu}(p,x)$	HPGe	$^{197}\text{Au}(p,n)^{197m}\text{Hg}, \sigma, \text{No. } 10, 5.5-13.9 \text{ MeV}$ $^{197}\text{Au}(p,n)^{197g}\text{Hg}, \sigma, \text{No. } 11, 4.5-13.9 \text{ MeV}$
(Satheesh et al., 2012)	Au foil 3.32 mg/cm ²	Cyclotron Stacked foil	Faraday cup	HPGe	$^{197}\text{Au}(p,n)^{197m}\text{Hg}, \sigma, \text{No. } 7, 8.43-20 \text{ MeV}$ $^{197}\text{Au}(p,n)^{197g}\text{Hg}, \sigma, \text{No. } 7, 8.43-20 \text{ MeV}$ $^{197}\text{Au}(p,n)^{197m}\text{Hg}^{197g}\text{Hg}, \sigma, \text{rat. No. } 7, 8.43-20 \text{ MeV}$
Tárkányi (2015) this work	Au foil	Cyclotron Stacked foil	$^{27}\text{Al}(p,x)^{22,24}\text{Na}$ $^{nat}\text{Ti}(p,x)^{48}\text{V}$	HPGe	$^{197}\text{Au}(p,n)^{197m}\text{Hg}, \sigma, \text{No. } 46, 7.24-63.48 \text{ MeV}$ $^{197}\text{Au}(p,n)^{197g}\text{Hg}, \sigma, \text{No. } 11, 7.25-25.2 \text{ MeV}$ $^{197}\text{Au}(p,3n)^{195m}\text{Hg}, \sigma, \text{No. } 40, 18.74-63.48 \text{ MeV}$ $^{197}\text{Au}(p,3n)^{195g}\text{Hg}, \sigma, \text{No. } 40, 18.74-63.48 \text{ MeV}$ $^{197}\text{Au}(p,5n)^{193m}\text{Hg}, \sigma, \text{No. } 24, 35.46-63.28 \text{ MeV}$ $^{197}\text{Au}(p,5n)^{193g}\text{Hg}, \sigma, \text{No. } 23, 33.95-63.48 \text{ MeV}$ $^{197}\text{Au}(p,6n)^{192g}\text{Hg}, \sigma, \text{No. } 20, 44.74-63.48 \text{ MeV}$ $^{197}\text{Au}(p,x)^{196m}\text{Au}, \sigma, \text{No. } 46, 11.97-63.48 \text{ MeV}$ $^{197}\text{Au}(p,x)^{196g}\text{Au}, \sigma, \text{No. } 48, 7.25-63.48 \text{ MeV}$ $^{197}\text{Au}(p,x)^{195}\text{Au}, \sigma, \text{No. } 35, 20.88-63.48 \text{ MeV}$ $^{197}\text{Au}(p,x)^{194}\text{Au}, \sigma, \text{No. } 44, 7.25-63.48 \text{ MeV}$ $^{197}\text{Au}(p,x)^{191}\text{Au}, \sigma, \text{No. } 7, 58.08-63.48 \text{ MeV}$ $^{197}\text{Au}(p,x)^{191}\text{Pt}, \sigma, \text{No. } 19, 37.95-63.48 \text{ MeV}$ $^{197}\text{Au}(p,x)^{192}\text{Ir}, \sigma, \text{No. } 19, 46.91-63.48 \text{ MeV}$

Table 2: Decay and nuclear characteristics of the investigated reaction products, contributing reactions and their Q-values

Nuclide Spin Isomeric level (keV)	Half-life	Decay path (%)	E_γ (keV)	I_γ (%)	Contributing process	Q-value (keV)
^{197m}Hg 13/2 ⁺ 298.93	23.8 h	EC 8.6 IT 91.4	133.98 279.01	33.5 6	$^{197}\text{Au}(p,n)$	-1681.22
^{197g}Hg 1/2 ⁻	64.14 h	EC 100	77.351 191.437	18.7 0.632	$^{197}\text{Au}(p,n)$ ^{197m}Hg decay	-1382.29
^{195m}Hg 13/2 ⁺ 176.07	41.6 h	EC 45.8 IT 54.2	261.75 387.87 560.27	31 2.18 7.1	$^{197}\text{Au}(p,3n)$	-17242.4
^{195g}Hg 1/2 ⁻	10.53 h	EC 100	180.11 207.1 261.75 585.13 599.66 779.80 1111.04 1172.38	1.95 1.6 1.6 2.04 1.83 7.0 1.48 1.28	$^{197}\text{Au}(p,3n)$ ^{195m}Hg decay	-17066.3
^{193m}Hg 13/2 ⁽⁺⁾ 140.765	11.8 h	IT 7.2 EC 92	257.99 407.63 573.26 932.57	49 32 26 12.5	$^{197}\text{Au}(p,5n)$	-33286.5
^{193g}Hg 3/2 ⁻	3.8 h	EC 100	186.56 381.60 861.11 1118.84	15.2 16 12.4 8.0	$^{197}\text{Au}(p,5n)$ ^{195m}Hg decay	-33145.7
^{192}Hg 0 ⁺	4.85 h	EC 100	157.2 274.8 306.5	7.2 52 5.5	$^{197}\text{Au}(p,6n)$	-40268.8
^{196m}Au 12 ⁻ 595.664	9.6 h	IT 100	137.69 147.81 168.37 188.27 285.49 316.19	1.3 43.5 7.8 30.0 4.4 3.0	$^{197}\text{Au}(p,pn)$	-8668.02
^{196g}Au 2 ⁻	6.1669 d	EC 93.0 β^- 7.0	333.03 355.73 426.10	22.9 87 6.6	$^{197}\text{Au}(p,pn)$ ^{196m}Au decay	-8072.36
^{195g}Au 3/2 ⁺	186.09 d	EC 100	98.88 129.757	11.2 0.842	$^{197}\text{Au}(p,p2n)$ ^{195m}Au decay ^{195}Hg decay	-14714.13
^{194}Au 1 ⁻	38.02 h	EC 100	293.548 328.464 1468.882	10.58 60.4 6.61	$^{197}\text{Au}(p,p3n)$ ^{194}Hg decay	-23141.77
^{191}Au 1 ⁻	3.18 h	EC 99.746 β^+ 0.254	277.86 399.84 586.44 674.22	6.4 4.2 15.0 6.0	$^{197}\text{Au}(p,p6n)$ ^{191}Hg decay	-45757.7
^{191}Pt 3/2 ⁻	2.83 d	ϵ 100	359.90 409.44 538.90	6.0 8.0 13.7	$^{197}\text{Au}(p,2p5n)$ ^{191}Au decay	-43085.08
^{192}Ir 4 ⁺	73.829 d	ϵ 4.76 β^- 95.24	295.95650 308.45507 316.50618 468.06885 604.41105	28.71 29.70 82.86 47.84 8.216	$^{197}\text{Au}(p,3p3n)$	-35095.22

When complex particles are emitted instead of individual protons and neutrons, the Q-values have to be decreased by the respective binding energies of the compound particles: np-d: +2.2 MeV; 2np-t: +8.48 MeV; 2p2n- α : +28.30 MeV

Table 3: Experimental cross sections of $^{197m}, ^{195m}, ^{195g}, ^{193m}, ^{193g}, ^{192}\text{Hg}$, $^{196m}, ^{196g}(\text{cum}), ^{195}\text{Au}(\text{cum})$, $^{194}, ^{191}(\text{cum})\text{Au}$, $^{191}(\text{cum})\text{Pt}$ and ^{192}Ir nuclear reactions (series 1, 2 and 3 are separated by thick lines)

Energy $E \pm \Delta E$	^{197m}Hg		^{197g}Hg		^{195m}Hg		^{195g}Hg		^{193m}Hg		^{193g}Hg		^{192}Hg		$^{196m}\text{Au}(\text{cum})$		^{196g}Au		$^{195}\text{Au}(\text{cum})$		^{194}Au		$^{191}\text{Au}(\text{cum})$		^{191m}Pt		^{192}Ir					
MeV	Cross section $\sigma \pm \Delta\sigma$ (mb)																															
63.5	0.3	3.8	0.5			47.6	5.2	31.6	4.2	112.0	12.4	43.1	5.7	464.8	50.3	10.8	1.3	151.6	16.4	275.7	29.9	147.3	15.9	186.5	20.5	146.4	15.9	0.41	0.05			
62.6	0.3	4.4	0.8			54.2	5.9	35.2	4.7	127.7	14.2	44.6	5.7	505.4	54.7	12.1	1.4	167.4	18.1	341.0	37.0	165.0	17.9	149.7	16.5	119.2	13.0	0.37	0.04			
61.7	0.4	3.5	0.6			47.6	5.2	30.4	4.4	124.3	13.9	44.5	5.6	494.4	53.5	8.1	1.0	145.5	15.7	266.9	28.9	141.9	15.4	99.0	11.0	76.5	8.3	0.35	0.04			
60.8	0.4	4.5	1.0			60.7	6.6	45.9	6.0	163.8	18.2	46.5	6.2	584.4	63.2	9.6	1.2	179.1	19.4	309.4	33.5	172.0	18.6	77.7	8.8	62.1	6.8	0.39	0.04			
59.9	0.4	3.9	0.8			58.8	6.4	46.0	5.6	171.3	18.8	45.7	5.8	563.1	60.9	9.2	1.1	167.2	18.1	316.9	34.3	160.6	17.4	51.1	6.0	38.8	4.3	0.38	0.04			
59.0	0.4	4.2	0.5			54.7	5.9	39.5	5.0	177.9	19.5	59.0	6.8	517.4	56.0	8.4	1.0	156.8	17.0	289.7	31.4	149.1	16.1	26.5	3.3	24.6	2.7	0.38	0.04			
58.1	0.5	3.9	1.0			56.3	6.1	48.8	6.2	194.4	21.4	53.2	6.1	464.5	50.3	8.4	1.0	151.1	16.4	287.7	31.2	148.0	16.0	13.4	1.8	14.6	1.6	0.32	0.04			
57.1	0.5	5.6	1.1			67.8	7.3	67.0	8.1	243.4	26.7	63.5	7.4	501.7	54.3	9.5	1.1	177.3	19.2	329.4	35.7	167.8	18.2			12.5	1.5	0.33	0.04			
56.2	0.5	4.9	1.0			68.1	7.4	74.4	8.6	277.8	30.3	74.2	8.3	446.7	48.3	8.9	1.1	178.6	19.3	286.3	31.0	167.3	18.1			0.4	0.5	0.25	0.03			
55.2	0.6	3.9	0.5			63.8	6.9	65.6	7.9	283.1	30.9	75.6	8.6	355.9	38.5	7.7	1.0	152.9	16.5	295.8	32.1	137.8	14.9					0.30	0.04			
54.2	0.6	3.7	1.1			67.8	7.3	87.5	10.1	328.4	35.8	86.8	9.7	307.0	33.2	9.3	1.1	167.1	18.1	316.3	34.3	154.2	16.7			10.2	1.2	0.29	0.03			
53.2	0.6	6.2	0.7			73.4	7.9	98.0	11.3	389.5	42.4	109.4	12.2	263.2	28.5	9.3	1.1	177.1	19.2	340.1	36.8	155.8	16.9					0.27	0.03			
52.2	0.7	7.0	0.8			71.6	7.7	100.2	11.8	407.2	44.4	122.2	13.6	192.4	20.8	10.0	1.2	171.6	18.6	345.9	37.5	145.4	15.7					0.24	0.03			
51.2	0.7	3.7	1.0			77.4	8.4	109.3	12.6	430.2	46.9	132.6	14.6	124.3	13.5	8.4	1.0	174.4	18.9	325.7	35.3	149.4	16.2			8.8	1.1	0.24	0.03			
50.2	0.7	4.4	0.9			77.9	8.4	101.4	11.8	420.9	45.9	129.1	14.2	74.2	8.0	7.5	0.9	169.3	18.3	336.0	36.4	139.1	15.1			8.8	1.0	0.18	0.02			
49.1	0.8	3.7	0.8			81.6	8.8	110.1	12.6	443.9	48.3	152.0	16.7	40.3	4.4	8.8	1.1	177.1	19.2	357.2	38.7	140.2	15.2			9.4	1.1	0.17	0.02			
48.0	0.8	5.5	0.7			90.7	9.8	114.7	13.1	502.3	54.8	150.8	16.6	17.2	1.9	10.7	1.3	177.1	19.2	362.4	39.3	131.9	14.3					0.17	0.02			
46.9	0.8	7.4	0.9			86.4	9.4	99.7	11.1	372.3	40.4	135.2	14.9	5.7	0.7	9.7	1.1	164.7	17.8	339.3	36.8	111.4	12.1			4.4	0.5	0.16	0.02			
47.1	0.3	8.0	1.8			65.4	7.1	51.2	6.2	367.8	39.8	154.7	17.2	4.7	0.5	5.7	0.9	167.0	18.1	353.3	38.5	110.7	12.0			9.9	1.1	0.12	0.03			
44.7	0.4	8.5	1.8			79.0	8.6	59.1	7.1	310.8	33.7	77.6	8.8	1.0	0.2			148.7	16.1	356.4	38.9	81.5	8.8			9.4	1.2					
42.6	0.4	8.0	1.2			101.9	11.0			92.8	10.1	25.4	3.0					5.1	0.6	166.4	18.0	364.2	40.0	68.7	7.4	11.6	1.3					
40.3	0.5	6.8	0.8			90.2	9.8	71.8	8.1	103.8	11.3	32.8	3.7					7.9	0.9	171.4	18.5	366.2	39.8	51.8	5.6			2.1	0.6			
37.9	0.6	6.8	0.7			163.1	17.7	71.9	7.9	18.0	2.0	5.9	0.7					6.9	0.8	170.6	18.5	400.4	190.7	25.8	2.8			1.3	0.2			
35.5	0.7	7.0	0.8			246.0	26.6	115.1	12.7	0.5	0.1							8.0	0.9	167.6	18.1	519.1	56.5	11.8	1.3							
32.8	0.8	9.4	1.0			413.1	44.7	160.2	17.4									5.8	0.6	159.6	17.3	731.2	79.7	5.7	0.6							
29.8	0.9	8.7	1.0			642.3	69.5	337.7	36.9									5.4	0.6	145.8	15.8	1006.8	109.3	2.7	0.3							
28.9	0.9	9.8	1.1			660.9	71.5	366.3	39.9									4.5	0.5	139.4	15.1	1230.8	133.3	2.6	0.3							
28.0	0.9	9.0	1.0			662.7	71.7	400.4	43.5									4.3	0.5	132.5	14.3	1013.9	311.8	2.1	0.2							
27.0	0.9	10.0	1.1			649.8	70.3	416.5	45.3									3.9	0.5	126.5	13.7	1272.7	137.9	1.6	0.2							
26.1	1.0	9.5	1.3			625.2	67.6	434.3	47.3									3.0	0.4	119.6	12.9	1277.7	138.4	1.2	0.2							
25.1	1.0	11.2	1.4			578.1	62.5	411.2	44.8									2.4	0.3	109.4	11.8	928.7	100.9	1.0	0.1							
24.1	1.0	10.9	1.4			522.0	56.5	383.2	41.8									1.9	0.3	99.5	10.8	1124.9	121.8	1.0	0.1							
23.1	1.1	9.8	1.2			431.7	46.7	350.2	38.2									1.7	0.3	85.3	9.2	934.6	101.2	0.74	0.09							
22.0	1.1	14.4	1.6			327.5	35.4	233.4	25.3									0.6	0.1	72.4	7.8	597.9	64.9	0.76	0.08							
20.9	1.1	11.0	1.2			215.8	23.4	177.2	19.2									0.6	0.1	59.2	6.4	501.1	54.5	0.71	0.09							
24.0	0.3	11.5	1.2	4.3	1.3	637.6	69.0	399.7	43.4									2.5	0.3	106.5	11.5	887.0	96.5	0.72	0.08							
22.1	0.4	11.7	1.3	7.9	2.9	512.1	55.4	358.8	38.9									1.1	0.2	87.6	9.5	690.1	75.5	0.54	0.07							
20.1	0.4	12.1	1.3	17.0	2.9	286.9	31.1	251.9	27.4									0.91	0.20	64.8	7.0	474.9	54.0	0.43	0.06							
18.8	0.5	11.7	1.3	14.6	2.0	98.6	10.7	115.0	12.5									0.26	0.08	43.4	4.7			0.14	0.02							
17.3	0.5	13.1	1.4	20.5	2.3	7.8	0.9	12.5	1.5									0.10	0.04	27.4	3.0			0.07	0.01							
15.7	0.6	16.6	1.8	27.0	2.9													0.05	0.01	11.4	1.2			0.06	0.01							
14.0	0.6	22.8	2.5	35.9	3.9													0.06	0.01	3.2	0.3			0.04	0.005							
12.2	0.7	35.1	3.8	62.1	6.7													0.05	0.01	0.93	0.10			0.03	0.004							
10.1	0.7	15.9	1.7	68.3	7.3													0.04	0.01	0.81	0.09			0.01	0.002							
7.7	0.8	4.4	0.5	48.4	5.2															0.80	0.09											
4.9	0.9	0.02	0.002	1.9	0.2															0.76	0.08											